GEORGIA INSTITUTE OF TECHNOLOGY
OFFICE OF CONTRACT ADMINISTRATION
SPONSORED PROJECT INITIATION

Date: February 26, 1981

Project Title: The Effects of Radomes and Polarizers on Polarimetric Processing Seekers

Project No: E-21-645

Project Director: Dr. G. K. Huddleston

Sponsor: Battelle Columbus Laboratories, Durham Operations; Research Triangle Park, N. C. 27709

Agreement Period: From 2/2/81 Until 8/2/81 (Perf.); 9/2/81 (Repts.)

Type Agreement: Delivery Order No. 1789 (Time & Materials Subcontract under ARO Prime Contract No. DAAG29-76-D-0100)

Amount: $10,710

Reports Required: Oral Reports as requested; Final Report

Sponsor Contact Person (s):

Technical Matters

Mr. Robert Russell
Advanced Sensors Directorate
U. S. Army Missile Laboratory
ATTN: DRSMI-REG
Redstone Arsenal, AL 35898
(205) 876-4061

Contractual Matters
(thru OCA)

Mr. L. G. Franklin
Administrative Officer
Scientific Services Program
Battelle Columbus Laboratories
Durham Operations
200 Park Drive
P. O. Box 12297
Research Triangle Park, N. C. 27709
(919) 549-8291

Defense Priority Rating: None

Assigned to: Electrical Engineering (School/~~Laboratory~~)

COPIES TO:

Project Director
Division Chief (EES)
School/Laboratory Director
Dean/Director—EES
Accounting Office
Procurement Office
Security Coordinator (OCA)
Reports Coordinator (OCA)

Library, Technical Reports Section
EES Information Office
EES Reports & Procedures
Project File (OCA)
Project Code (GTRI)
Other OCA Research Property Coordinator

CA-3 (3/76)

GEORGIA INSTITUTE OF TECHNOLOGY OFFICE OF CONTRACT ADMINISTRATION

SPONSORED PROJECT TERMINATION SHEET

Date 12/9/81

Project Title: The Effects of Radomes and Polarizers on Polarimetric Processing Seekers

Project No: E-21-645

Project Director: Dr. G. K. Huddleston

Sponsor: Battelle Columbus Labs; Durham Operations

Effective Termination Date: 9/2/81

Clearance of Accounting Charges: 10/2/81 (report period)

Grant/Contract Closeout Actions Remaining:

- [x] Final Invoice and Closing Documents *
- [ ] Final Fiscal Report
- [x] Final Report of Inventions
- [x] Govt. Property Inventory & Related Certificate
- [ ] Classified Material Certificate
- [ ] Other _____

*Grants & Contracts Accounting please send "duplicate original" of the STAS Claims Voucher - Final

Assigned to: Electrical Engineering (School/~~Laboratory~~)

COPIES TO:

Administrative Coordinator	Research Security Services	EES Public Relations (2)
Research Property Management	~~Reports Coordinator (OCA)~~	Computer Input
Accounting	Legal Services (OCA)	Project File
Procurement/EES Supply Services	Library	Other _____

FORM OCA 10:781

GTA

E21-645

Final Technical Report

THE EFFECTS OF RADOMES AND POLARIZERS ON POLARIMETRIC PROCESSING SEEKERS

By

Gene K. Huddleston

Submitted to

U. S. ARMY MISSILE LABORATORY
DRSMI–REG
REDSTONE ARSENAL, ALABAMA

Under

Scientific Services Program
Delivery Order No. 1789
Prime Contract DAAG29–76–D–0100
Battelle Columbus Laboratories

October 1981

GEORGIA INSTITUTE OF TECHNOLOGY
A UNIT OF THE UNIVERSITY SYSTEM OF GEORGIA
SCHOOL OF ELECTRICAL ENGINEERING
ATLANTA, GEORGIA 30332

1981

UNCLASSIFIED

SECURITY CLASSIFICATION OF THIS PAGE *(When Data Entered)*

REPORT DOCUMENTATION PAGE

READ INSTRUCTIONS BEFORE COMPLETING FORM

1. REPORT NUMBER	2. GOVT ACCESSION NO. / 3. RECIPIENT'S CATALOG NUMBER
4. TITLE *(and Subtitle)* The Effects of Radomes and Polarizers on Polarimetric Processing Seekers	5. TYPE OF REPORT & PERIOD COVERED Final Report 2 Feb. 1981 - 2 Sept. 1981
	6. PERFORMING ORG. REPORT NUMBER E-21-645
7. AUTHOR(s) Gene K. Huddleston	8. CONTRACT OR GRANT NUMBER(s) DAAG29-76-D-0100
9. PERFORMING ORGANIZATION NAME AND ADDRESS School of Electrical Engineering Georgia Institute of Technology Atlanta, Georgia 30332	10. PROGRAM ELEMENT, PROJECT, TASK AREA & WORK UNIT NUMBERS Delivery Order 1789
11. CONTROLLING OFFICE NAME AND ADDRESS DRSMI-REG Redstone Arsenal, AL 35898	12. REPORT DATE November 1981 13. NUMBER OF PAGES 44 pages
14. MONITORING AGENCY NAME & ADDRESS *(if different from Controlling Office)* Battelle Columbus Laboratories Durham Operations Research Triangle Park, NC 27709	15. SECURITY CLASS. *(of this report)* UNCLASSIFIED 15a. DECLASSIFICATION/DOWNGRADING SCHEDULE

16. DISTRIBUTION STATEMENT *(of this Report)*

17. DISTRIBUTION STATEMENT *(of the abstract entered in Block 20, if different from Report)*

18. SUPPLEMENTARY NOTES

19. KEY WORDS *(Continue on reverse side if necessary and identify by block number)*

Radome analysis; polarimetric radar

20. ABSTRACT *(Continue on reverse side if necessary and identify by block number)*

A polarimetric radar model is presented which incorporates the radome into the analysis. Polarimetric scattering models are developed whose statistical properties replicate those reported in the literature. The results of computer-aided simulations are presented which assess the performance of seven radar processing schemes, polarimetric and otherwise.

DD FORM 1 JAN 73 1473 EDITION OF 1 NOV 65 IS OBSOLETE

UNCLASSIFIED

SECURITY CLASSIFICATION OF THIS PAGE *(When Data Entered)*

THE EFFECTS OF RADOMES AND POLARIZERS

ON

POLARIMETRIC PROCESSING SEEKERS

Final Technical Report, Project E-21-645

by

Gene K. Huddleston
School of Electrical Enigneering
Georgia Institute of Technology
Atlanta, Georgia 30332

for

Robert Russell
U.S. Army Missile Laboratory
DRSMI-REG
Redstone Arsenal, Alabama 35898

under

Scientific Services Program
Battelle Columbus Laboratories
Durham Operations

Delivery Order 1789
DAAG29-76-D-0100

November 1981

TABLE OF CONTENTS

CHAPTER I

INTRODUCTION

This report presents the results of research to analyze the effects of radomes and polarizers on the performance of polarimetric processing seekers operating against targets in ground clutter. The ultimate objective is to identify radome and polarizer configurations which may lead to improved tracking performance.

Efforts described in this report have been directed to the development of a tractable mathematical model of a polarimetric processing radar which includes the effects of the radome (or polarizer) on multiple radar returns (in angle) from the same range cell. Such a model has been developed as described in Chapter 2.

The model developed has been used to establish some baseline performance characteristics for the case of no radome (polarizer). Computer-aided simulations have been carried out using the radar model and the scattering models described in Chapter 2. The simulations have been restricted to the case of sum mode reception only; i.e., effects of polarimetric processing in angle tracking within a given range cell have yet to be assessed. The results of the simulations for seven processing schemes are presented in Chapter 3.

Conclusions and recommendations for future work are presented in Chapter 4.

This research has been carried out under the Scientific Services Program through Battelle Columbus Laboratories, Durham Operations, under Delivery Order 1789 of Contract DAAG29-76-D-0100.

The helpful discussions with Lloyd W. Root and Robert Russell, Advanced Sensors Directorate, U.S. Army Missile Laboratory, Redstone Arsenal, Alabama, are gratefully acknowledged.

CHAPTER 2

ANALYSIS METHODS

2.1 Overview of Radar Model

The narrow-band voltage $V_R(t)$ received by a radome-enclosed, polarimetric radar antenna channel can be written using complex envelope techniques and Lorentz reciprocity [1] as

$$V_R(t) = -\frac{Z_G Z_T}{V_T(Z_G + Z_T)} \left(\sum_{p=1}^{N} \int_{S_{ap}} [\underline{E}_T \times \underline{H}'_{Rp} - \underline{E}'_{Rp} \times \underline{H}_T] \cdot \hat{Z} dxdy \right) e^{j2\pi f_c t} \qquad (1)$$

where the summation is taken over the returns $\underline{E}'_{Rp}$, $\underline{H}'_{Rp}$ from all N scatterers lying within a given resolution cell, and where

Z_G = Internal impedance of transmitter

Z_T = Input impedance to the antenna

V_T = Voltage at antenna terminals when transmitting

$\underline{E}_T, \underline{H}_T$ = Aperture fields of antenna when transmitting with the receiver polarization state (sum, elevation difference, or azimuth difference modes)

$\underline{E}'_{Rp}, \underline{H}'_{Rp}$ = Fields incident on antenna aperture when receiving as produced by backscatterer from targets and clutter after traversing the radome and or polarizer.

The operating frequency is f_c. The antenna aperture lies in the xy-plane at z=0. Unit vectors are denoted by carets (^). For seeker antennas, the received voltage for any one of three monopulse modes ($\Sigma, \Delta_{EL}, \Delta_{AZ}$) can be obtained by using the corresponding aperture illuminations $(\underline{E}_T, \underline{H}_T)_\Sigma$, $(\underline{E}_T, \underline{H}_T)_{\Delta EL}$, and $(\underline{E}_T, \underline{H}_T)_{\Delta AZ}$ in Equation (1).

Other radar system parameters are embodied in the following expression for the target return from the p^{th} scatterer prior to traversing the radome or polarizer [2,3]:

$$\underline{E}_{Rp} = \sqrt{\frac{P_T G_T}{4\pi r_p^2}}\ \underline{S}_p \cdot \hat{h}_T(\hat{k}_p)\ \mu\left(t - \frac{2r_p}{c}\right) e^{j2\pi\nu_p t}\ e^{-j2\pi \frac{2r_p}{c}} \qquad (2)$$

where

$\mu(t)$ = Waveform of the transmitted pulse

$\hat{h}_T(\hat{k}_p)$ = complex unit vector which describes the polarization of the transmitted fields in elevation ($\hat{\varepsilon}$) and azimuth ($\hat{\alpha}$) components

$$\underline{S}_p = \frac{1}{\sqrt{4\pi r_p^2}} \begin{bmatrix} \sqrt{\sigma_{hh}}\, e^{j\phi_{hh}} & \sqrt{\sigma_{hv}}\, e^{j\phi_{hv}} \\ \sqrt{\sigma_{vh}}\, e^{j\phi_{vh}} & \sqrt{\sigma_{vv}}\, e^{j\phi_{vv}} \end{bmatrix} = \text{Polarization Scattering Matrix}$$

c = Velocity of wave propagation

ν_p = Doppler frequency

$G_T(\hat{k}_p)$ = Gain of the transmitting antenna in direction $\hat{k}_p$

P_T = Transmitted power

r_p = Distance from transmitting antenna to the scatterer.

The target return from each scatterer is a TEM wave incident on the radome (or polarizer). The radome affects the incident wave in a manner such as to cause amplitude and phase variations in the wavefront as it traverses the dielectric shell; hence, it is desirable in such analysis to use the receiving formulation presented in Equation (1) rather than a simpler formulation valid for the case of no radome.

In the present investigation, attention has focused on the polarization properties of the radar returns from resolution cells which contain

clutter only, target and clutter, and decoy and clutter. For each such cell, it is necessary to define a coordinate system which facilitates the use of Equations (1) and (2) in regard to the complex vector fields and polarization vectors defined therein. A spherical coordinate system centered about the transmitting antenna is chosen for this purpose. The xy plane coincides with the antenna aperture. The z-axis is normal to the aperture and centered in it. The line-of-sight to the p^{th} scatterer is denoted by the unit vector $\hat{k}_p$ at spherical angles θ_p and ϕ_p; equivalently, $\hat{k}_p$ can be denoted by its direction cosines (k_{xp},k_{yp},k_{zp}). Unit vectors $\hat{\varepsilon},\hat{\alpha}$ -- orthogonal to each other and to $\hat{k}_p$ -- are defined in Figure 2-1(a) and used to quantify the vector nature of the fields: the elevation direction $\hat{\varepsilon}$ denotes vertical polarization for fields incident on each scatterer, and the azimuth direction $\hat{\alpha}$ denotes horizontal polarization. A resolution cell is defined in Figure 2-1(b).

The second term in the integrand of Equation (1) can be omitted with no significant change in the received voltage for returns within the main beam of the aperture antenna. Also, $\underline{H}'_{Rp} \approx (\underline{E}'_{Rp} \times \hat{k}_p)/\eta$. When these approximations are combined with the vectors $\hat{\varepsilon}$, $\hat{\alpha}$ defined above, there results

$$V_R(t) = -\frac{e^{j2\pi f_c t} Z_G Z_T}{V_T(Z_G+Z_T)} \sum_{p=1}^{N} \sqrt{\frac{P_T G_T}{4\pi r_p^2}} \int_{S_{ap}} \left[E_{Tx} E'_{\alpha p} \sqrt{1-k_{yp}^2} - E_{Ty} \left(\frac{k_{zp} E'_{\varepsilon p} + k_{xp} E'_{\alpha p}}{\sqrt{1-k_{yp}^2}} \right) \right] dxdy \qquad (3)$$

where $E'_{\varepsilon p}$, $E'_{\alpha p}$ are the elevation and azimuth components of the scattered fields <u>at the antenna</u> as given by

$$\begin{bmatrix} E'_{\alpha p} \\ E'_{\varepsilon p} \end{bmatrix} = \underline{S}_p \begin{bmatrix} h_{T\alpha p} \\ h_{T\varepsilon p} \end{bmatrix} \mu\left(t - \frac{2r_p}{c}\right) e^{j2\pi\nu_p t} \; e^{-j2\pi \frac{2r_p}{c}} \qquad (4)$$

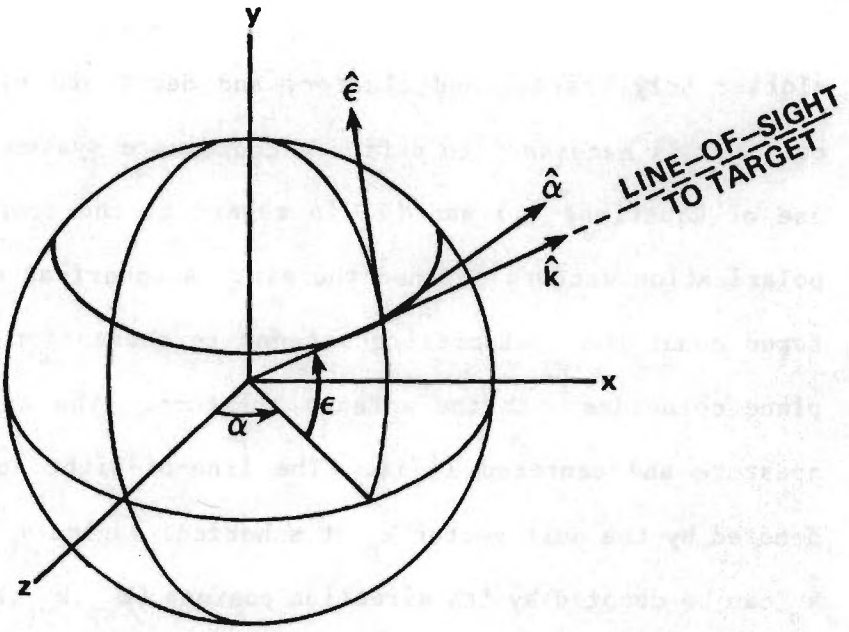

(a) Elevation–Azimuth Coordinate System

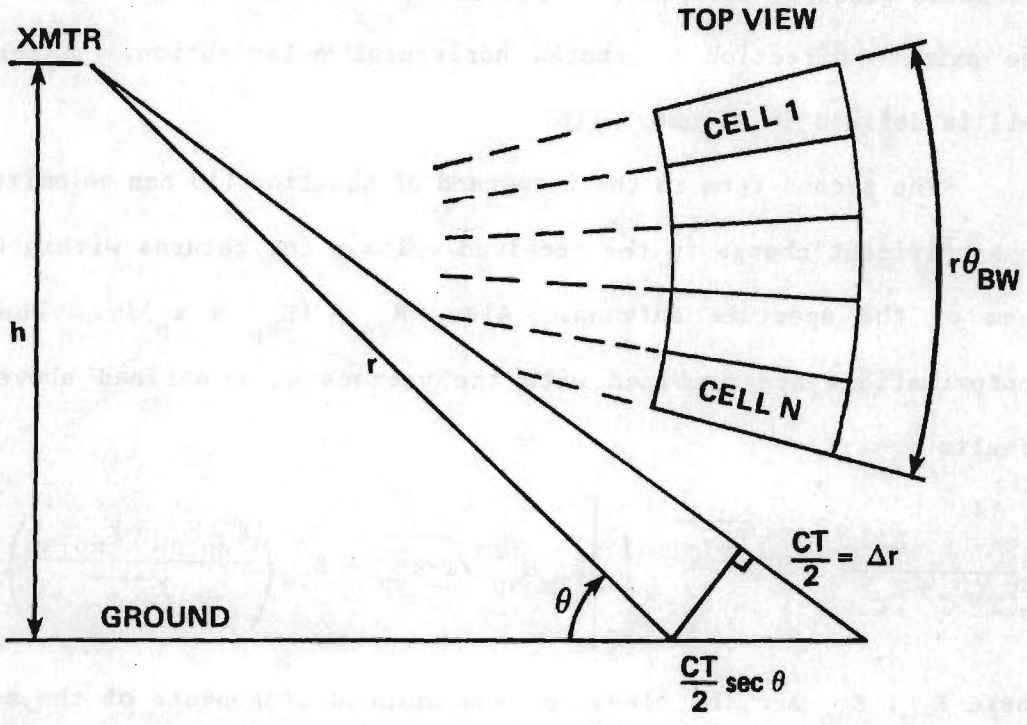

(b) Geometry for Range Resolution

FIGURE 2–1. COORDINATE SYSTEMS FOR RADAR MODEL.

In Equation (4), $h_{T\alpha p}$, $h_{T\epsilon p}$ denote the polarization of the field incident on the scatterer with polarization scattering properties defined by matrix $\underline{S}_p$. The vector

$$\hat{h}_T = \hat{\alpha} h_{T\alpha p} + \hat{\epsilon} h_{T\epsilon p} \tag{5}$$

is a unit vector, and the amplitude of the incident field on each scatterer is given by the $(P_T G_T / 4\pi r_p^2)^{\frac{1}{2}}$ factor in Equation (3). The polarization scattering matrix $\underline{S}$ is given, after Barton [3], in terms of radar cross-section by

$$\underline{S} = \frac{1}{\sqrt{4\pi r^2}} \begin{bmatrix} \sqrt{\sigma_{11}}\, e^{j\phi_{11}} & \sqrt{\sigma_{12}}\, e^{j\phi_{12}} \\ \sqrt{\sigma_{21}}\, e^{j\phi_{21}} & \sqrt{\sigma_{22}}\, e^{j\phi_{22}} \end{bmatrix} \tag{6}$$

Properties of $\underline{S}$ are discussed in the next section.

Orthogonal, linearly polarized channels can be provided on the antenna to separate the horizontal (x) component from the vertical (y) component of received signal, the effect of which is to perform the aperture integration in two independent parts corresponding to the two terms in the integrand of Equation (3). Equation (3) may be rewritten using complex envelope techniques [4] as is appropriate for narrow-band signal analysis; i.e.,

$$E_h(t) = V_n(t) e^{j2\pi f_c t} = V_{ho}(t) e^{j\phi_h(t)}\, e^{j2\pi f_c t} \tag{7a}$$

$$E_v(t) = V_v(t) e^{j2\pi f_c t} = V_{vo}(t) e^{j\phi_v(t)}\, e^{j2\pi f_c t} \tag{7b}$$

where $V_h(t)$ and $V_v(t)$ are the complex envelopes and are slowly varying with respect to cos $2\pi f_c t$. If these signals are passed through a square law detector (SLD) consisting of a scaled squaring circuit followed by an ideal low-pass filter which effectively blocks frequencies near f_c [5], then the outputs are

$$V_H^2(t) = \frac{a\, V_{ho}^2(t)}{2} \tag{8a}$$

$$V_V^2(t) = \frac{a\, V_{vo}^2(t)}{2} \tag{8b}$$

where a is the scaling constant. For convenience in later analysis, the scaling constant may be set to a=2 and a square root may be taken to yield

$$V_H(t) = V_{ho}(t) \tag{9a}$$

$$V_V(t) = V_{vo}(t) \tag{9b}$$

Hence, $V_H(t)$, $V_V(t)$ are the amplitudes of the envelopes of the signals given in Equations (3) and (7).

The envelopes $V_{ho}(t)$, $V_{vo}(t)$ contain all of the radar information embodied in the return from the various resolution cells at different ranges as designated by the time delay $2r_p/c$. The polarization scattering matrix $\underline{S}_p$ accounts for the amplitude, phase, and polarization of the field scattered monostatically from each resolution element when the incident field is specified by $\hat{h}_T$. Random variations in phase due to random variations in r_p and doppler frequency ν_p are accounted for by the exponential terms within the summations of Equations (4).

Of particular interest is the resulting difference in phase between the signals received in the horizontal and vertical channels as given by

$$\frac{V_h(t)}{V_v(t)} = \frac{|V_h(t)|}{|V_v(t)|} e^{j(\phi_n - \phi_v)} = \frac{V_{ho}}{V_{vo}} e^{j\beta_{HV}} \tag{9}$$

This phase angle β_{HV} is of paramount importance in polarimetric processing and depends on the sum of the effects of scattering from N resolution cells in a statistical manner; such scattering is the subject of a later section.

2.2 Polarization Scattering Matrix

A polarization scattering matrix [6-13] approach is used to model scattering from each resolution cell. One form of the polarization scattering matrix gives the voltages received in orthogonal polarization channels when the target is illuminated by these orthogonal polarizations. When the chosen polarizations are horizontal and vertical, the received voltages at the antenna terminals (before detection) are given by

$$V_h = C \begin{bmatrix} 1 \\ 0 \end{bmatrix}^T \begin{bmatrix} S_{hh} & S_{hv} \\ S_{vh} & S_{vv} \end{bmatrix} \begin{bmatrix} E_h \\ E_v \end{bmatrix} = C(S_{hh}E_h + S_{hv}E_v) \tag{10a}$$

$$V_v = C \begin{bmatrix} 0 \\ 1 \end{bmatrix}^T \begin{bmatrix} S_{hh} & S_{hv} \\ S_{vh} & S_{vv} \end{bmatrix} \begin{bmatrix} E_h \\ E_v \end{bmatrix} = C(S_{vh}E_h + S_{vv}E_v) \tag{10b}$$

wher C is a complex constant and T denotes matrix transpose, and where

S_{hh} = (voltage received on horizontal channel when horizontal polarization is transmitted)/C

S_{hv} = (voltage received on horizontal channel when vertical polarization is transmitted)/C

S_{vh} = (voltage received on vertical channel when horizontal polarization is transmitted)/C

S_{vv} = (voltage received on vertical channel when vertical polarization is transmitted)/C

The incident field is given in vector notation and in matrix notation by

$$\underline{E}_i = \hat{h}E_h + \hat{v}E_v = \begin{bmatrix} E_h \\ E_v \end{bmatrix} = \sqrt{\frac{P_T G_T}{4\pi r^2}} \begin{bmatrix} h_h \\ h_v \end{bmatrix} \tag{11}$$

where $\hat{h},\hat{v}$ are unit vectors orthogonal to each other and to the line-of-sight between the transmitting/receiving radar antenna and target.

In general,

$$V_{||} = C \begin{bmatrix} 1 \\ 0 \end{bmatrix}^T \underline{S}' \begin{bmatrix} E_{||} \\ E_{\perp} \end{bmatrix} \tag{12a}$$

$$V_{\perp} = C \begin{bmatrix} 0 \\ 1 \end{bmatrix}^T \underline{S}' \begin{bmatrix} E_{||} \\ E_{\perp} \end{bmatrix} \tag{12b}$$

where

$$\underline{S}' = \begin{bmatrix} S_{|| \, ||} & S_{|| \, \perp} \\ S_{\perp \, ||} & S_{\perp \, \perp} \end{bmatrix} = \begin{bmatrix} S_{11} & S_{12} \\ S_{21} & S_{22} \end{bmatrix} \tag{13}$$

The incident field can be written as

$$\underline{E}_i = \hat{a}_{||} E_{||} + \hat{a}_{\perp} E_{\perp} \tag{14}$$

where $E_{||}$, $E_{\perp}$ are orthogonal polarizations; e.g., horizontal and vertical,

left circular and right circular, or any other pair as easily determined on the Poincaire' sphere as antipodal points as illustrated in Figure 2-2(a).

Transformations of the scattering matrix $\underline{S}$ for one set of orthogonal polarizations to $\underline{S}'$ for another set can be accomplished as follows [7,8]:

$$\underline{S}' = \underline{R}^T(\psi)\ \underline{H}^T(\tau)\ \underline{S}\ \underline{H}(\tau)\ R(\psi) \tag{15}$$

where

$$\underline{R}(\psi) = \begin{bmatrix} \cos\psi & -\sin\psi \\ \sin\psi & \cos\psi \end{bmatrix} \tag{16a}$$

$$\underline{H}(\tau) = \begin{bmatrix} \cos\tau & j\sin\tau \\ j\sin\tau & \cos\tau \end{bmatrix} \tag{16b}$$

The operation $\underline{R}^T(\psi)\ \underline{S}\ \underline{R}(\psi)$ represents rotation of the target about the line of sight as an axis through the angle ψ, where a positive angle ψ represents a left-handed rotation (i.e., counterclockwise looking in the direction to the target from the transmitter). Such relative rotation between the antenna and target about the line of sight results in the new matrix

$$\underline{S}' = \underline{R}^T(\psi)\ \underline{S}\ \underline{R}(\psi) \tag{17}$$

where the elements of $\underline{S}$ and $\underline{S}'$ represent the voltages that would be measured by orthogonal linear polarizations before and after rotation of the target relative to the antenna.

$$r = a^2 = E_{\parallel}^2 + E_{\perp}^2$$

$$\theta = \pi/2 - 2\tau$$

$$\phi = 2\psi$$

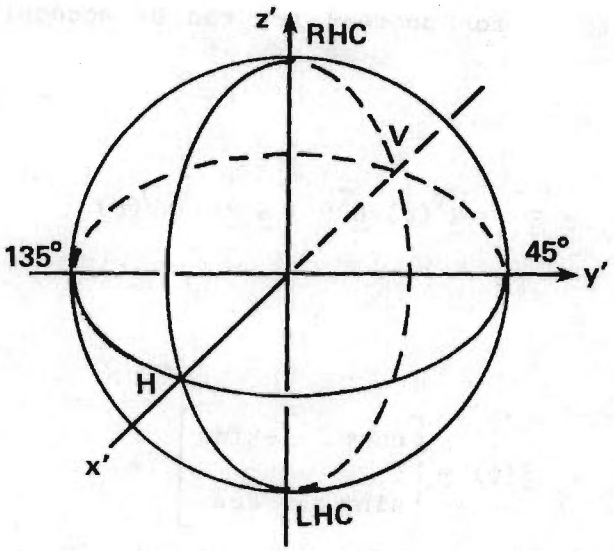

(a) Poincaire' Sphere

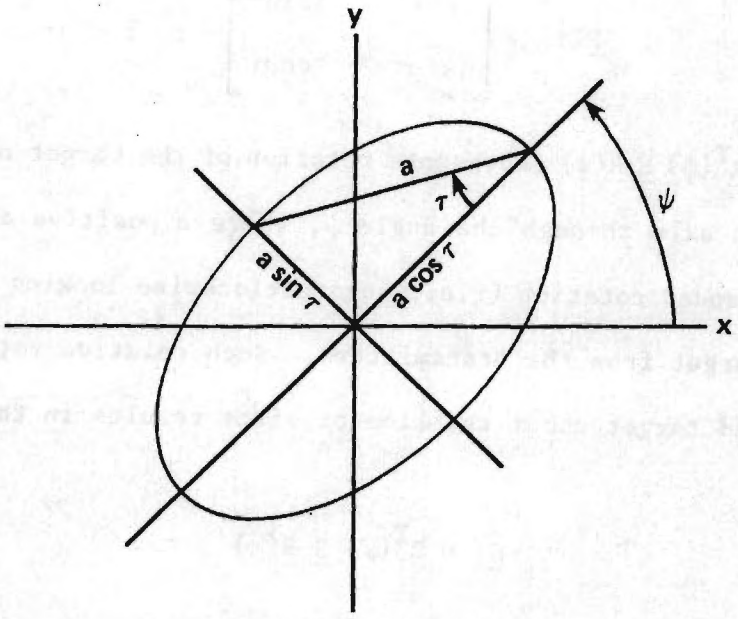

(b) Rotated Polarization Ellipse

FIGURE 2–2. POINCAIRE SPHERE AND POLARIZATION ELLIPSE.

For example, consider the elemental object scattering matrix $\underline{S}$ for a horizontal dihedral with horizontal and vertical transmit and receive polarizations [7]:

$$\underline{S} = C \begin{bmatrix} 1 & 0 \\ 0 & -1 \end{bmatrix} \tag{18}$$

The diagonal terms are zero because the dihedral has a horizontal plane of symmetry. Rotate the dihedral through the angle $\psi = \pi/2$ to obtain a vertical dihedral. The scattering matrix $\underline{S}'$ for the vertical dihedral is given by

$$\underline{S}' = R^T(\psi)\underline{S}\,\underline{R}(\psi) = C \begin{bmatrix} \cos 2\psi & -\sin 2\psi \\ -\sin 2\psi & -\cos 2\psi \end{bmatrix}_{\psi=\frac{\pi}{2}} = C \begin{bmatrix} -1 & 0 \\ 0 & 1 \end{bmatrix} \tag{19}$$

for horizontal and vertical orthogonal polarizations used in transmit and receive. The diagonal terms are again zero because the vertical dihedral also has a horizontal plane of symmetry. The voltages received for 45° linear transmission from a dihedral at angle ψ are given by Equations (10) and the general form of $\underline{S}'$ above; viz.,

$$V_h = C \begin{bmatrix} 1 \\ 0 \end{bmatrix}^T \begin{bmatrix} \cos 2\psi & -\sin 2\psi \\ -\sin 2\psi & -\cos 2\psi \end{bmatrix} \begin{bmatrix} 1/\sqrt{2} \\ 1/\sqrt{2} \end{bmatrix} = C \frac{\cos 2\psi - \sin 2\psi}{\sqrt{2}} \tag{20a}$$

$$V_v = C \begin{bmatrix} 0 \\ 1 \end{bmatrix}^T \begin{bmatrix} \cos 2\psi & -\sin 2\psi \\ -\sin 2\psi & -\cos 2\psi \end{bmatrix} \begin{bmatrix} 1/\sqrt{2} \\ 1/\sqrt{2} \end{bmatrix} = C \frac{-\sin 2\psi - \cos 2\psi}{\sqrt{2}} \tag{20b}$$

where C is the complex constant which embodies the range, etc. For $\psi=0$ (horizontal dihedral), the polarization of the received wave is -45° linear; for $\psi = \pi/2$, the polarization of the received wave is +135° linear. These results are, of course, well known and are presented to help clarify the procedures described.

Assume next that the orthogonal polarizations of the antenna were right-hand circular (RHC) and left-hand circular (LHC). The voltages received in these two channels for, say, RHC transmit can be determined from Equations (12) if the scattering matrix $\underline{S}'$ indicated in Equation (13) is known, where $\|$ corresponds to RHC and $\perp$ to LHC. The required matrix $\underline{S}'$ can be found from the transformation of $\underline{S}$ given in Equation (19) for h-v polarizations according to

$$\underline{S}' = \underline{H}^T(\tau)\, \underline{S}\, \underline{H}(\tau) \qquad (21)$$

for $\tau = \pm\pi/4$ for circular polarizations. The ellipticity operator $\underline{H}$ changes the axial ratio of antenna polarization while maintaining the major axes of the orthogonal polarization ellipses along the $\hat{x}=\hat{h}$, $\hat{y}=\hat{v}$ axes.

The ellipticity angle τ is illustrated in Figure 2-2(b) for the general case of the rotated polarization ellipse as embodied in the general transformation of Equation (15). The relationships between the ellipse parameters and coordinates on the Poincaire' sphere are given in Figure 2-2(a) for convenient reference. The Poincaire' coordinates of RHC polarization are $(\theta=0,\phi)$; hence, $\tau = \pi/4$ for RHC. Similarly, $\tau = -\pi/4$ for LHC polarization.

Returning to the example where $\tau = -\pi/4$, there results

$$\underline{S}' = \frac{C}{\sqrt{2}} \begin{bmatrix} 1 & -j \\ -j & 1 \end{bmatrix}^T \begin{bmatrix} -1 & 0 \\ 0 & 1 \end{bmatrix} \frac{1}{\sqrt{2}} \begin{bmatrix} 1 & -j \\ -j & 1 \end{bmatrix} = C \begin{bmatrix} -1 & 0 \\ 0 & 1 \end{bmatrix} \tag{22}$$

(The same result is also obtained for $\tau = \pi/4$.) The new matrix $\underline{S}'$ is used in the following way. Let a RHC wave be transmitted by the antenna. The return from the vertical dihedral should also be RHC since it is an even bounce reflector. The received voltages are given formally by

$$V_{RHC} = C \begin{bmatrix} 1 \\ 0 \end{bmatrix}^T \begin{bmatrix} -1 & 0 \\ 0 & 1 \end{bmatrix} \begin{bmatrix} E_{RHC} \\ 0 \end{bmatrix} = -C\, E_{RHC} \tag{23a}$$

$$V_{LHC} = C \begin{bmatrix} 0 \\ 1 \end{bmatrix}^T \begin{bmatrix} -1 & 0 \\ 0 & 1 \end{bmatrix} \begin{bmatrix} E_{RHC} \\ 0 \end{bmatrix} = 0 \tag{23b}$$

where the minus sign in Equation (23a) is due to inversion of the horizontal component of incident field as it is reflected by the vertical dihedral.

It is worthwhile to state the general result for converting the h-v polarization scattering matrix $\underline{S}$ to the corresponding matrix $\underline{S}'$ for RHC/LHC polarizations:

$$\underline{S}' = \underline{H}^T(\pi/4) \begin{bmatrix} S_{hh} & S_{hv} \\ S_{vh} & S_{vv} \end{bmatrix} \underline{H}(\pi/4) = \begin{bmatrix} S_{RR} & S_{RL} \\ S_{LR} & S_{LL} \end{bmatrix} \tag{24a}$$

where

$$S_{RR} = \frac{S_{hh} - S_{vv}}{2} + j\, S_{hv} \tag{24b}$$

$$S_{RL} = j\, \frac{S_{hh} + S_{vv}}{2} \tag{24c}$$

$$S_{LL} = \frac{S_{vv} - S_{hh}}{2} + j\, S_{hv} \tag{24d}$$

It is noted that post multiplication of $\underline{S}$ by $\underline{H}(\pi/4)$ yields a matrix which quantifies the received voltages in h-v channels when illumination is by RHC or LHC. Premultiplication of $\underline{S}$ by $\underline{H}^T(\pi/4)$ yields a matrix which quantifies the received voltages in RHC/LHC channels when illumination is horizontal or vertical. Other pairs of orthogonal polarizations can also be accommodated by proper selection of τ in the pre- and post-multiplications. For all such transformations, it is noted that the quantity (see Equation (13))

$$P = |S_{11}|^2 + |S_{22}|^2 + 2|S_{12}|^2 \tag{25}$$

is invariant since it represents conservation of power [8].

It is also noted that for any fixed scatterer (target), there exist two orthogonal pairs (four in all) of optimal polarizations such that maximum power is received by the transmit/receive antenna in one case, and minimum power is received in the other. The "maximum" polarization is found by determining the polarization scattering matrix wherein the cross-polarized elements S_{12}, S_{21} vanish. The pair of orthogonal transmit/receive polarizations which achieve this condition comprise two distinct, antipodal (diametrically opposed) points on the Poincaire' sphere, and are called cross-polarization (x-pol) nulls. The "minimum" polarization is found by determining the polarization scattering matrix wherein the co-polarized elements S_{11}, S_{22} vanish. The pair of orthogonal polarizations which achieve this condition also comprise two distinct points on the Poincaire' sphere, and are called the co-polarization (co-pol) nulls. The

four polarization nulls all lie on one great circle of the polarization sphere, and the angle between radii to the co-pol nulls is bisected by the diameter line joining the x-pol nulls. For example, x-pol nulls for a vertical dihedral are located at $\theta=0$ and $\theta=\pi$ on the Poincaire' sphere, since either RHC or LHC transmit/receive polarizations result in maximum received power and yield $S_{12} = S_{21} = 0$. The co-pol nulls are given by ($\theta = \pi/4$, $\phi = \pm\pi/2$) since 45° linear or 135° linear transmit/receive polarizations result in minimum (zero!) received power because of the 90° twist imparted to the linear polarization by the vertical dihedral.

Given a polarization scattering matrix $\underline{S}$, the co-pol and x-pol nulls are defined by solutions of [10]

$$\text{Co-pol:}\quad S_{11} + \rho_c^2 S_{22} + 2\rho_c S_{12} = 0 \tag{26a}$$

$$\text{X-pol:}\quad -\rho_x^* S_{11} + \rho_x S_{22} + S_{12}(1 - \rho_x \rho_x^*) = 0 \tag{26b}$$

where * denotes complex conjugation. Since each equation is quadratic in ρ_c or ρ_x, there are two solutions to each. The variables are related to the coordinates (θ,ϕ) on the Poinciare' sphere by

$$\theta = \frac{\pi}{2} - 2\tau = \text{Cot}^{-1}\left\{\frac{q - q^*}{j(1 - qq^*)}\right\} \tag{27a}$$

$$\phi = \text{Tan}^{-1}\left\{\frac{j(q + q^*)}{q - q^*}\right\} \tag{27b}$$

where the quantity q is defined by

$$q = \frac{1 - j\rho}{1 + j\rho} \tag{28}$$

Under certain conditions of target symmetry, degenerate solutions may occur.

The elements of the polarization scattering matrix were related to radar cross-sections in Equation (6), which is the unifying concept needed to connect the presentation in Section 2.1 to that in this section. Thus, it is apparent that the elements of $\underline{S}$ depend on target orientation and frequency of operation. In the applications which consider randomly oriented, complex targets in ground clutter, the elements of $\underline{S}$ must be considered as stochastic quantities as discussed in the next section.

2.3 Scattering Models

Each resolution cell defined in Figure 2-1(b) is considered to contain clutter only, clutter and target, or clutter and decoy (such as a dihedral or flat plate). Root [14] describes the salient polarimetric scattering properties of such cells as shown in Figure 2-3. Left-hand circular (LHC) polarization is transmitted by the antenna, and the radar returns are received separately on orthogonal, linearly polarized channels. The phase angle β_{HV} is defined to be that between the signal received on the horizontal channel and the signal received on the vertical channel as presented in Equation (9) earlier. The probability density functions shown in Figure 2-3 represent the relative frequency of occurence of $\sin \beta_{HV}$, and were obtained by observing approximately 1000 actual pulse returns from cells whose contents are described in the figure.

The interpretation of the data in Figure 2-3 elucidates the concept of polarimetric radar. When clutter is illuminated by a LHC polarized field, the scattering process is such as to return fields that are mostly elliptically polarized -- and almost none that are circularly polarized ($\sin \beta_{HV} = \pm 1$). When LHC fields impinge on a dihedral in clutter, the

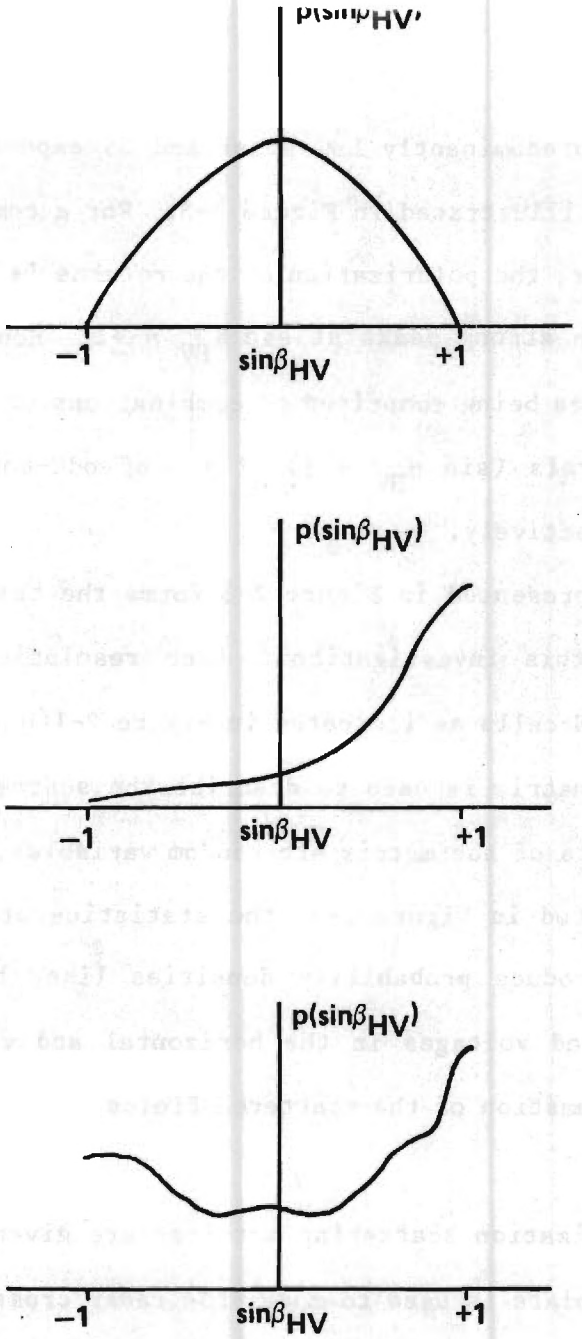

FIGURE 2–3. PROBABILITY DENSITY FUNCTIONS OF POLARIMETRIC PHASE OF BACKSCATTER FROM TARGETS IN GROUND CLUTTER ILLUMINATED WITH LHC.

radar return is predominantly LHC polarized as expected for a two bounce reflector and as illustrated in Figure 2-3. For a complex target (such as a tank) in clutter, the polarization of the returns is distributed over the spectrum but with strong peaks at $\sin \beta_{HV} = \pm 1$. Hence, such targets are often thought of as being comprised of combinations of flat plates ($\sin \beta_{HV} = -1$) and dihedrals ($\sin \beta_{HV} = 1$); i.e., of odd-bounce and even-bounce reflectors, respectively.

The data presented in Figure 2-3 forms the basis of the scattering models used in this investigation. Each resolution cell in range is subdivided into N cells as indicated in Figure 2-1(b). A single polarization scattering matrix is used to describe the scattering from each cell, where the elements of the matrix are random variables. For the three types of cells designated in Figure 2-3, the statistics of the matrix elements are chosen to produce probability densities like those in that figure, where the received voltages in the horizontal and vertical channels are computed as a summation of the scattered fields from N such cells according to Equation (3).

The polarization scattering matrices are given in Figure 2-4. For clutter, a flat plate is used to model the radar cross-section σ_c, and the polarization characteristics are chosen to bias the phases of the back-scattered fields as given by the probability density function (pdf) in the fourth column. The shape of $p(\psi)$ is cosine, and the parameter α is used to control the range of ψ. When $\alpha=0$, the deterministic case is obtained, and $\beta_{HV} = 0$ as indicated in the last two columns for Type 1. For the simulations to be described below, $\alpha = \pi/2$ was used.

For a dihedral in clutter, a pdf centered on $\pi/2$ with cosine variation was chosen as shown in Figure 2-4. The radar cross-section σ_D of the

TYPE	SCATTERER	POLARIZATION SCATTERING MATRIX [S] FOR LHC ILLUMINATION*	PROBABILITY DENSITY FUNCTION	PHYSICAL MODEL	SCATTERED FIELD $\underline{E}_S$ AT RECEIVER*	ψ	β_{hv}
1	CLUTTER	$\frac{\lambda\sqrt{\sigma_c}}{4\pi r^2}\begin{bmatrix}-1 & 0\\ 0 & -e^{-j\psi}\end{bmatrix} e^{j\phi_c}$ $\sqrt{\sigma_c} = \frac{2\sqrt{\pi}\sqrt{\sigma_0 A_c}}{\lambda}\frac{\sin(2\pi\frac{\sqrt{\sigma_0 A_c}}{\lambda}\sin\psi)}{(\frac{2\pi\sqrt{\sigma_0 A_c}}{\lambda}\sin\psi)}\cos\psi$	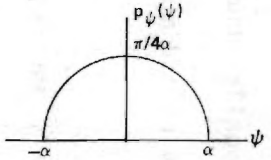	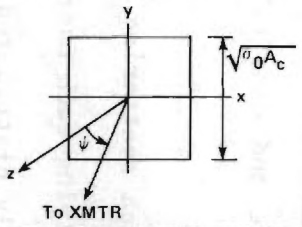	$-E'_0(\hat{h}+\hat{v})$	0	0
2	DIHEDRAL	$\frac{\lambda\sqrt{\sigma_D}}{4\pi r^2}\begin{bmatrix}-1 & 0\\ 0 & -e^{-j\psi}\end{bmatrix} e^{j\phi_D}$ $\sqrt{\sigma_D} = \frac{4\sqrt{\pi}ab\,\sin(\psi/4+3\pi/8)}{\lambda}$	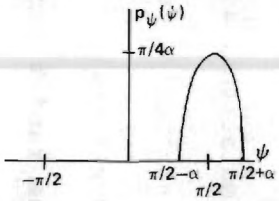	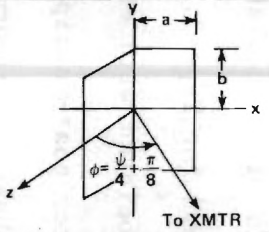	$-E'_0(\hat{h}+\hat{v}e^{-j\pi/2})$	$\pi/2$	$\pi/2$
3	TARGET	$\frac{\lambda\sqrt{\sigma_D}}{4\pi r^2}\begin{bmatrix}-1 & 0\\ 0 & -e^{-j\psi}\end{bmatrix} e^{j\phi_D}$ $\sqrt{\sigma_D} = \frac{4\sqrt{\pi}ab\,\sin(\psi/4+3\pi/8)}{\lambda}$	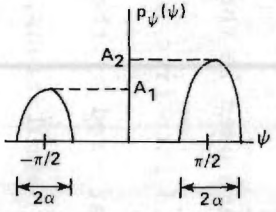	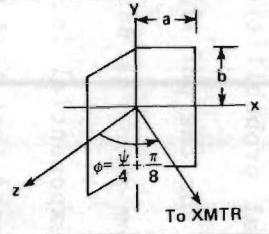	$-E'_0(\hat{h}+\hat{v}e^{-j\pi/2})$ $-E'_0(\hat{h}+\hat{v}e^{j\pi/2})$	$\pi/2$ $-\pi/2$	$\pi/2$ $-\pi/2$

* Polarization Scattering matrix and scattered fields are expressed in transmitter coordinates; i.e., $\underline{E}_s = [S]\cdot\begin{bmatrix}E_0\\ E_0 e^{j\pi/2}\end{bmatrix}$

Figure 2-4. Scattering Models Used in Polarimetric Radar Simulation.

dihedral is that given by Ruck [6, Volume 2, p. 589]. The phase properties are also those of a dihedral; i.e., an even-bounce reflector. For α=0, the deterministic case is obtained, and $\beta_{HV} = \pi/2$ as expected for this ideal scatterer. In the simulations $\alpha = \pi/2$ was used.

The scattering model for a target in clutter is shown under Type 3 in Figure 2-4. It is the same as that for the dihedral except that the pdf is bimodal: for ψ near $\pi/2$, the target looks like a dihedral; for α near $-\pi/2$, the target resembles a flat plate. In the simulations, $\alpha = \pi/2$ was used, and equal probabilities of flat plate and dihedral were imposed; i.e., $A_1 = A_2$ for the pdf shown for Type 3.

A random phase is associated with each scattering matrix as indicated by the exponential factor post-multiplying each matrix in Figure 2-4. It is assumed that this phase is uniformly distributed on the interval $(0,2\pi)$ for each scattering matrix. Typically, five clutter cells and one target cell were used in the simulations; additionally, the target cell was further divided into five more scattering centers to add more randomness to the fields scattered by the target cell.

In the simulations, the random variable ψ was generated using a random number generator available on the computing system and the method described by Conner [15]. A random number x, uniformly distributed on (0,1), is generated and used to compute ψ according to

$$\psi = P^{-1}(x) \tag{29}$$

where P^{-1} denotes the inverse of the probability distribution given by

$$P_{\psi}(\psi) = \int_{-\infty}^{\psi} p(\psi) d \tag{30}$$

and where $p_\psi(\psi)$ is the appropriate pdf given in Figure 2-4. When these pdf's are integrated, the resulting inverse functions are given by

$$\text{CLUTTER:} \quad \psi = \frac{2\alpha}{\pi} \sin^{-1}(2x - 1) \tag{31a}$$

$$\text{DIHEDRAL:} \quad \psi = \frac{2\alpha}{\pi} \sin^{-1}(2x - 1) + \frac{\pi}{2} \tag{31b}$$

$$\text{TARGET:} \quad \psi = \begin{cases} \frac{2\alpha}{\pi} \sin^{-1}\left(\frac{2x}{p_1} - 1\right) - \frac{\pi}{2}, & 0 \leq x \leq .5 \quad (31c) \\ \frac{2\alpha}{\pi} \sin^{-1}\left(\frac{2(x-p_1)}{p_2} - 1\right) + \frac{\pi}{2}, & .5 < x \leq 1.0 \quad (31d) \end{cases}$$

where

P_1 = Probability of flat plate

P_2 = Probability of dihedral.

In Figure 2-4, A_1 and A_2 are related to P_1 and P_2 by

$$A_1 = \frac{\pi p_1}{4\alpha} \tag{32a}$$

$$A_2 = \frac{\pi p_2}{4\alpha} \tag{32b}$$

It is emphasized that the scattering models have been heuristically derived with the objective that when they are used in a polarimetric radar simulation, the pdf's shown in Figure 2-3 will be closely replicated by the results of the simulation. The simulation consists of computing the complex envelopes given in Equations (7) for a large number of pulses (say, 4000) and for various relative cross-sections of clutter and target. Two such cases of interest are presented in Figure 2-5. Left-hand circular

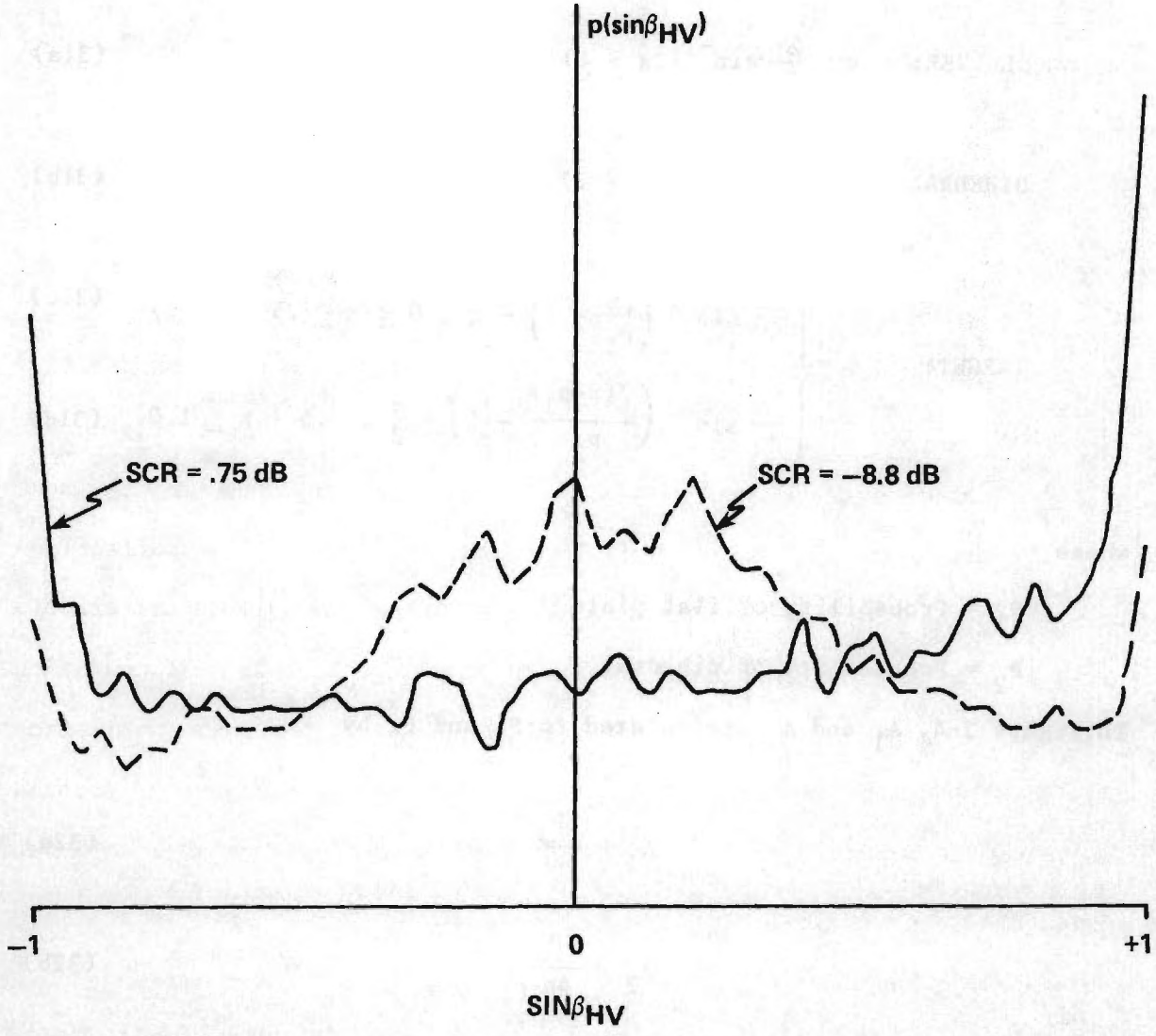

FIGURE 2–5. PROBABILITY DENSITY FUNCTION OF $SIN\beta_{HV}$ FOR TWO SIGNAL–TO–CLUTTER RATIOS.

polarization was used to illuminate five clutter cells with $\sqrt{\sigma_c} = 1.0$ and five target cells, each with $\sqrt{\sigma_T} = 0.2$, resulting in a signal-to-clutter ratio (SCR) of -8.8 dB. For the SCR = .75 dB case, $\sqrt{\sigma_T} = 0.6$ was used. The signal-to-clutter ratio is defined by

$$SCR = 10 \log_{10} \frac{E\{V_H^2 + V_V^2 \mid \text{Target only}\}}{E\{V_H^2 + V_V^2 \mid \text{Clutter only}\}} \tag{33}$$

where V_h, V_v are the received voltages in the horizontal and vertical antenna channels. Comparison of Figures 2-3 and 2-5 indicate that the scattering model replicates the measured data to a reasonable degree of accuracy.

Computational speed and simplicity of the simulation are two more objectives of the scattering models. It is realized that large collections of one- and two-bounce scatterers have been used in past simulation efforts with less than enormous success [14], and that large amounts of computation time are required to carry out the simulations. The computation time required to generate each curve in Figure 2-5 is approximately 50 seconds on the Cyber 70 system; in addition, the pdf's and performances of seven different radar processing schemes are also obtained as described in the next chapter.

It is also realized that better models are available for the radar cross-sections of targets and ground clutter. For example, it is commonly accepted that the amplitude of ground clutter can be described as the sum of a fixed and a random component [16], or as the sum of a diffuse and specular component [2, Ch. 11]. Other theoretical models utilize statistical clutter models such as the Rayleigh or Weibull probability distributions to model the backscatterer coefficient $\sigma_o = \sigma_c/A$, where A is the area illuminated. More intense models consider the physical composition of the

scattering bodies in the illuminated volume [6, Ch. 9], the results of which should fit some statistical description that, once identified, would suffice to describe the clutter in subsequent applications. Correlation of clutter returns and the dependence on frequency of the power spectra [3, pp. 98-100] should also be included in a complete clutter model so that the effects of frequency agility, processing time, receiver badnwidth, variable pulse duration, and pulse repetition rate can be properly accounted for.

Good statistical models of the radar cross sections of complex targets are also available. For amplitude fluctuations, Swerling's [17] four models which utilize Rayleigh distributions are well known and used as described by Barton [3, pp. 80-83]. Other important factors, such as angle glint and range glint can also be included. Unfortunately, no well-known polarimetric scattering models for either clutter or complex targets at frequencies of interest are presently available.

CHAPTER 3

SIMULATION RESULTS

3.1 Description of the Simulation

A digital computer simulation of seven polarimetric processing radars was carried out on a Cyber 70 computing system using the scattering models described in Figure 2-4. The objective of the simulation was to gain insight into the operation of polarimetric processing so that optimum processing schemes may become intuitively obvious, that the necessary tools would be developed for later investigations of angle tracking (monopulse) algorithms, and that the beneficial use of polarizers or spatial filters may be indicated.

The receiver models used in the simulation are presented in block diagram form in Figure 3-1. In all cases, the resolution cell was illuminated with LHC polarization. Each range cell was subdivided into 5 clutter cells, one of which may or may not contain a target or decoy. Scattering from each clutter cell was described by the polarimetric scattering matrix in Figure 2-4 (Type 1) where $\alpha = \pi/2$ and $\sqrt{\sigma_c} = 1.0$. Scattering from the cell containing a target was described by subdividing the cell into 5 subcells, each of which scattered the incident field according to the target polarization scattering matrix presented in Figure 2-4 (Type 3), where $\alpha = \pi/2$ and $.2 \leq \sqrt{\sigma_T} \leq .6$ to produce SCR's in the range -8.8 dB to .75 dB. The backscattered returns were received by a two-channel (h-v), linearly polarized antenna as indicated by the two separate terms in Equation (2-3) which are indicated in Figure 3-1 and in Equations (2-7) by E_H and E_V.

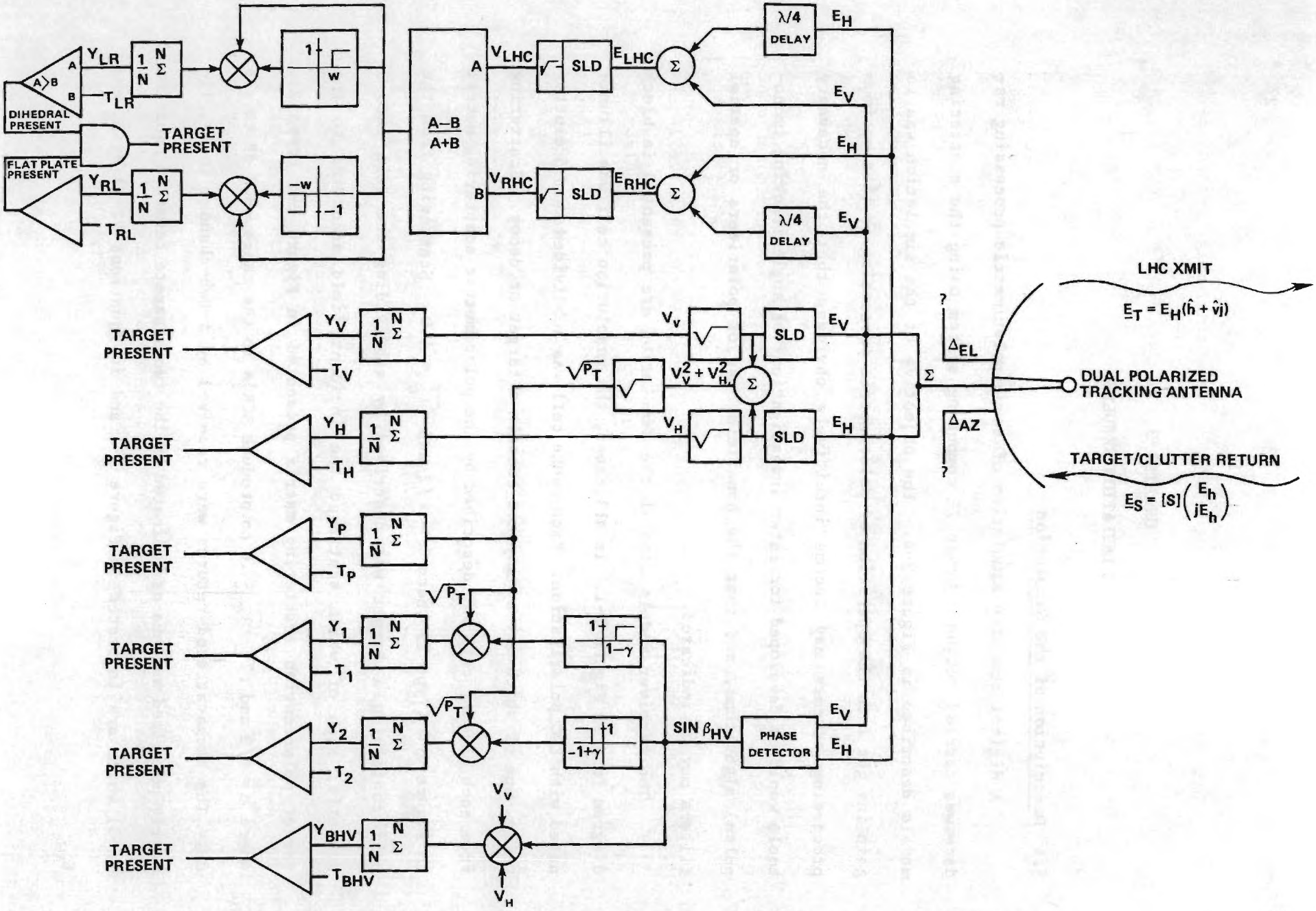

FIGURE 3–1. RECEIVER MODELS USED IN SIMULATION OF POLARIMETRIC PROCESSING SEEKERS.

Conventional (i.e., no polarimetric processing) radar processing is shown in the central part of Figure 3-1 to produce the outputs y_V, y_H, and y_P shown at the left side. The narrow-band signals E_H and E_V are passed through the square law detectors (SLD) to yield the real envelopes V_H^2 and V_V^2 of Equations (2-8). These variables are further processed to yield V_V, V_H, and P_T as shown in Figure 3-1. Signal averaging is next done for N samples to produce the random variables y_V, y_H, and y_P which are compared to appropriately set thresholds T_V, T_H and T_P to indicate target detection. The three models simulate radar target detection based on horizontally polarized backscatter only, vertical only, and total backscatter.

Three polarimetric processors are shown in the lower portion of Figure 3-1. The received signals E_H and E_V are applied to a phase detector which computes the discriminant $\sin \beta_{HV}$ as defined in Equation (2-9). In one case, the quantity $V_V V_H |\sin \beta_{HV}|$ is integrated to form variable y_{BHV}. In the second and third cases, P_T is multiplied by either unity or zero, depending on whether $\sin \beta_{HV} > (1-\gamma)$ or $\sin \beta_{HV} < (-1+\gamma)$ as indicated in the figure. The resulting outputs are averaged to form y_1 and y_2 as shown. The outputs of the two comparators would then be used together to indicate the presence of a target ($y_1 > T_1$ and $y_2 > T_2$), a dihedral ($y_1 > T_1$ only) or flat plate ($y_2 > T_2$ only). The rationale for this processor is that returns which produce $|\sin \beta_{HV}| < \gamma$ are due primarily to clutter and should be excluded and, hence, enhance the SCR of the detected signal.

Another polarimetric processor is shown in the upper portion of Figure 3-1. Quarter-wave delays are introduced in E_H and E_V as shown to produce signals E_{LHC} and E_{RHC} as received by a dual polarized, circularly polarized antenna. The real envelopes V_{LHC} and V_{RHC} are then processed according to

$$V = \frac{V_{LHC} - V_{RHC}}{V_{LHC} + V_{RHC}} \qquad (1)$$

The variable V is windowed, limited, and integrated as shown to produce the outputs y_{LR} and y_{RL}. Target detection is indicated when both outputs exceed their respective thresholds. The rationale for this processor is essentially the same as that for the "sin β_{HV}" processor.

The statistics of each variable defined in Figure 3-1 before averaging were computed using 4000 sample radar returns. The y variables were obtained by averaging 40 samples; hence, 100 samples of the integrated (averaged) variables were obtained.

3.2 Results

The computed probability density functions of the random variable sin β_{HV} were presented in Figure 2-5 for two signal-to-clutter ratios. These pdf's represent the statistics of the output of the phase detector in Figure 3-1.

Figure 3-2 presents the statistics of the variable P_T in terms of the relative distribution of signal power and clutter power versus sin β_{HV}. For the higher SCR of .75 dB, there is not a great deal of difference between the distributions except at the sin β_{HV} = 1 extreme. For the lower SCR of -8.8 dB, however, a greater difference is observed in the two distributions; in fact, the clutter distribution closely resembles that observed by Root as presented earlier in Figure 2-3.

Figure 3-3 examines the relative distribution of signal power and clutter power as a function of the window width γ, where γ=1 corresponds to a wide open window that allows all the power to enter. Figure 3-3 shows plots of

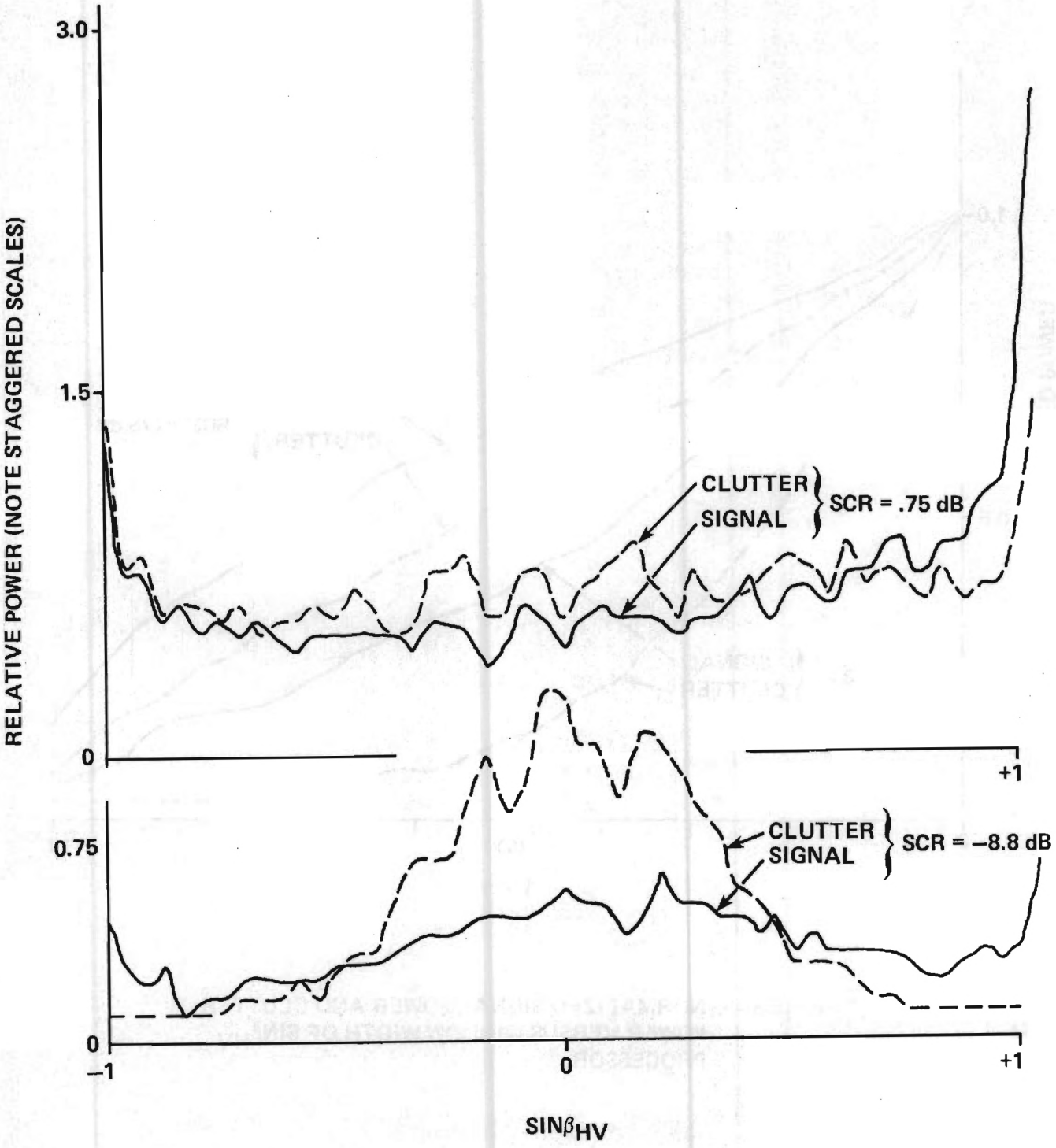

FIGURE 3–2. RELATIVE DISTRIBUTIONS OF SIGNAL POWER AND CLUTTER POWER VS. SINβ_{HV} FOR TWO SIGNAL–TO–CLUTTER RATIOS.

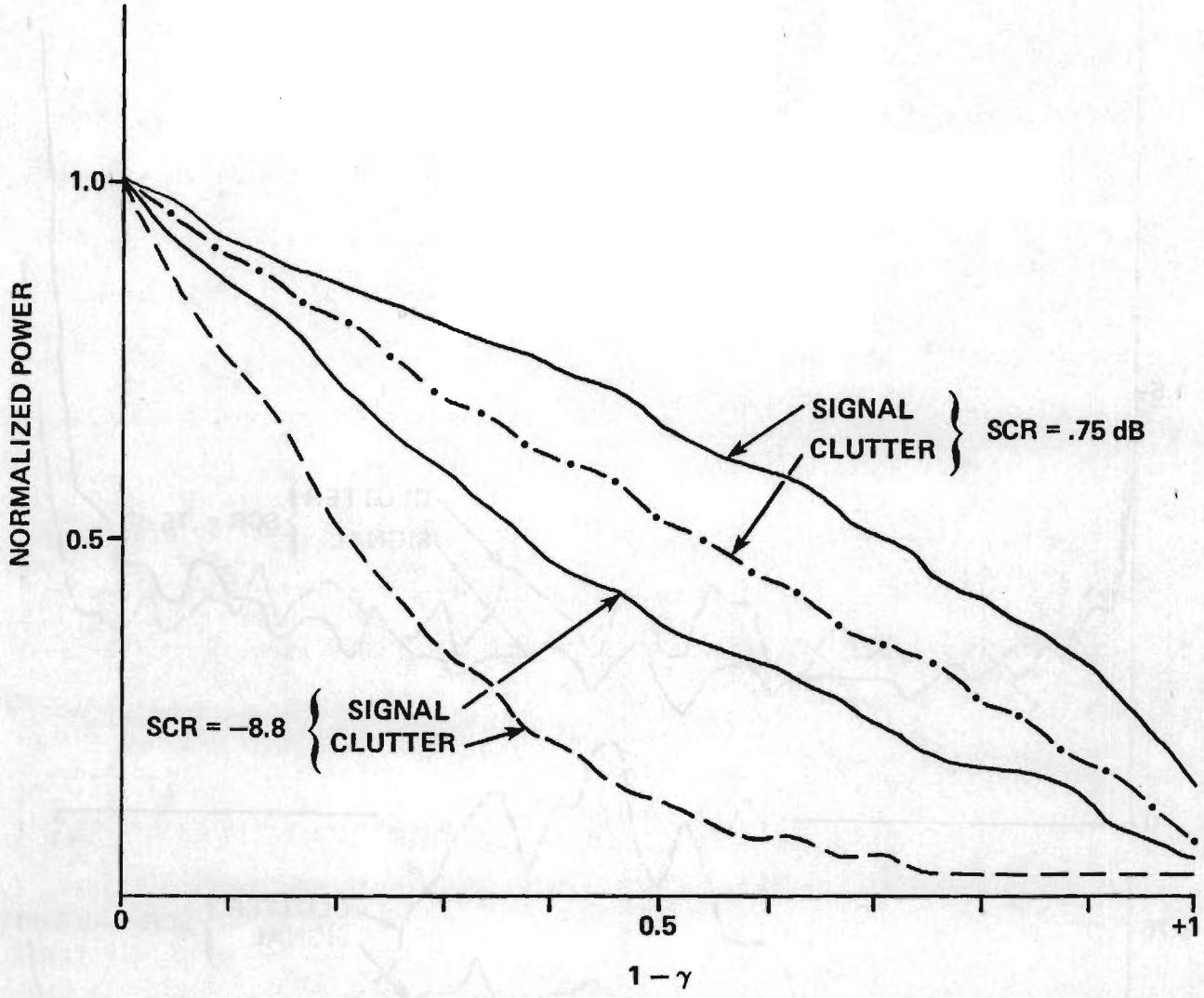

FIGURE 3–3. NORMALIZED SIGNAL POWER AND CLUTTER POWER VERSUS WINDOW WIDTH OF SINβ_{HV} PROCESSOR.

$$P(1-\gamma) = \frac{\int_{-1}^{-(1-\gamma)} P(\sin\beta_{HV})d(\sin\beta_{HV}) + \int_{1-\gamma}^{1} P(\sin\beta_{HV})d(\sin\beta_{HV})}{\int_{-1}^{1} P(\sin\beta_{HV})\, d(\sin\beta_{HV})} \qquad (2)$$

where $P(\sin\beta_{HV})$ is the relative distribution of power (signal or clutter) shown in Figure 3-2. These plots show that the difference between normalized signal power and clutter power increases with decreasing window width γ; furthermore, the difference is more pronounced for small SCR. One would conclude that a enhancement of SCR by controlling γ would be more effective at low SCR's than at high ones.

The SCR's of -8.8 dB and .75 dB cited in Figures 3-2 and 3-3 are the overall ratios computed according to Equation (2-33) using 4000 returns, or independent samples. Figures 3-4 and 3-5 show the relative distributions of the SCR on a pulse-by-pulse basis for the two overall SCR's of -8.8 dB and .75 dB. For the SCR of -8.8 dB, the most probably pulse-to-pulse SCR (50% point) is approximately -12 dB for the conventional power variables; however, it is approximately +12 dB for the $\sin\beta_{HV}$ processor. A similar improvement is shown in Figure 3-5 for the overall SCR of .75 dB.

The curves in the two figures were computed by examining the signals at the inputs of the integrators in Figure 3-1 for the cases of clutter only and target only. For example, the $\sin\beta_{HV}$ processor is shown as the lower most processor in Figure 3-1. The input to the integrator is $V = V_V V_H |\sin\beta_{HV}|$. The pulse-to-pulse SCR is defined by

$$\text{scr} = \frac{|V_t|^2, \text{ target only}}{|V_c|^2, \text{ clutter only}} \qquad (3)$$

These relative distributions show a definite enhancement of the scr due to polarimetric processing using the $\sin\beta_{HV}$ discriminant.

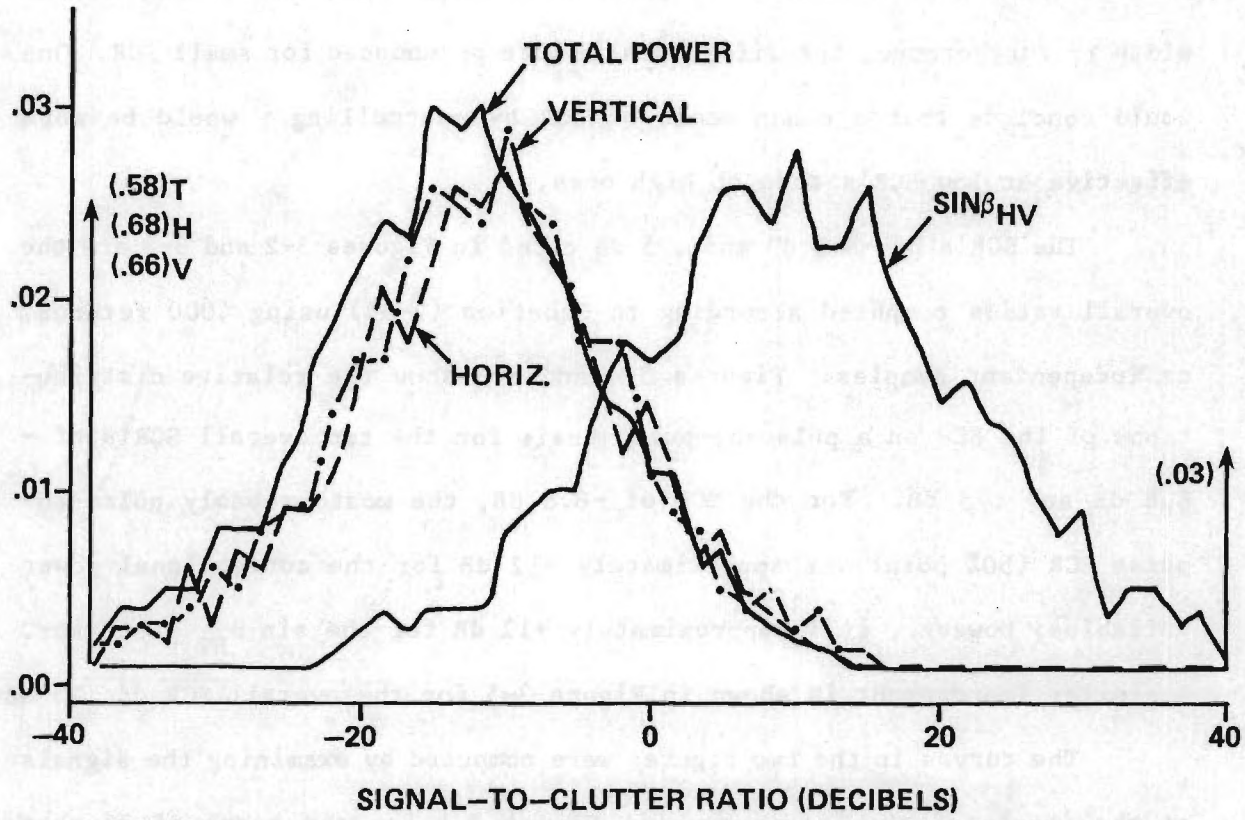

FIGURE 3–4. PROBABILITY DENSITY FUNCTIONS OF SIGNAL–TO–CLUTTER RATIO FOR RECEIVED POWER IN HORIZONTAL, VERTICAL, TOTAL, AND $SIN\beta_{HV}$ CHANNELS FOR AVERAGE SCR = –8.8 dB.

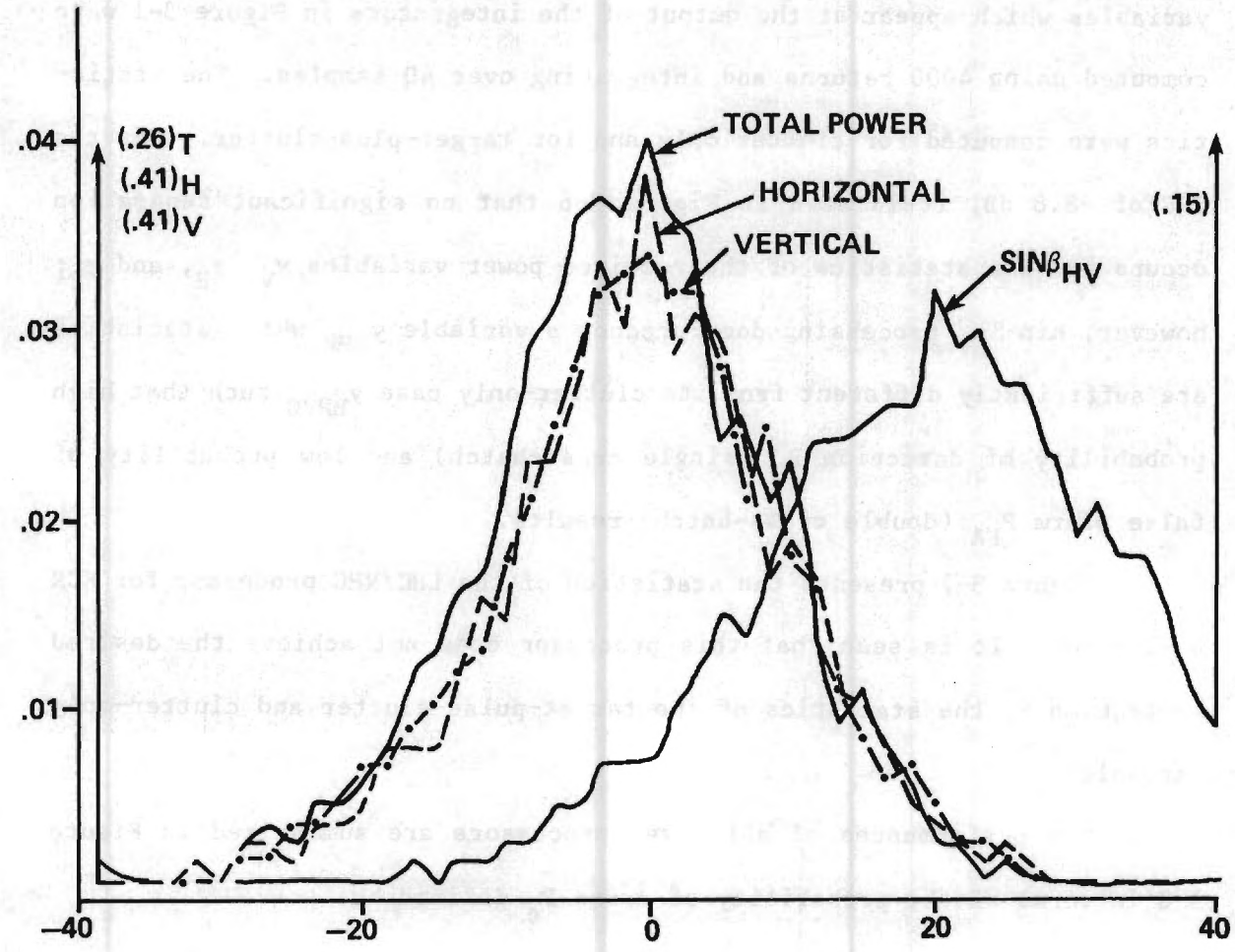

FIGURE 3–5. PROBABILITY DENSITY FUNCTIONS OF SIGNAL–TO–CLUTTER RATIO FOR POWER IN HORIZONTAL, VERTICAL, TOTAL POWER, AND $SIN\beta_{HV}$ CHANNELS FOR AVERAGE SCR = +.75 dB.

Figure 3-6 further elucidates the target detection process and illustrates the advantages of the sin β_{HV} processor. The pdf's of the random variables which appear at the output of the integrators in Figure 3-1 were computed using 4000 returns and integrating over 40 samples. The statistics were computed for clutter only and for target-plus-clutter. For the SRC of -8.8 dB, it is seen in Figure 3-6 that no significant separation occurs for the statistics of the received power variables y_V, y_H, and y_P; however, sin β_{HV} processing does produce a variable y_{BHV} whose statistics are sufficiently different from its clutter-only case y_{BHVC} such that high probability of detection P_D (single cross-hatch) and low probability of false alarm P_{FA} (double cross-hatch) results.

Figure 3-7 presents the statistics of the LHC/RHC processor for SCR = -8.8 dB. It is seen that this processor does not achieve the desired separation in the statistics of the target-pulse-clutter and clutter-only variables.

The performances of all seven processors are summarized in Figure 3-8 in terms of the probability of error P_e defined by

$$P_e = p\{y > T \mid \text{Target absent}\} + p\{y < T \mid \text{Target present}\} \qquad (4)$$

For the data here, the probability of a target being present was set to 0.5 to give

$$P_e = .5\, P_{FA} + .5\, (1-P_D) \qquad (5)$$

where

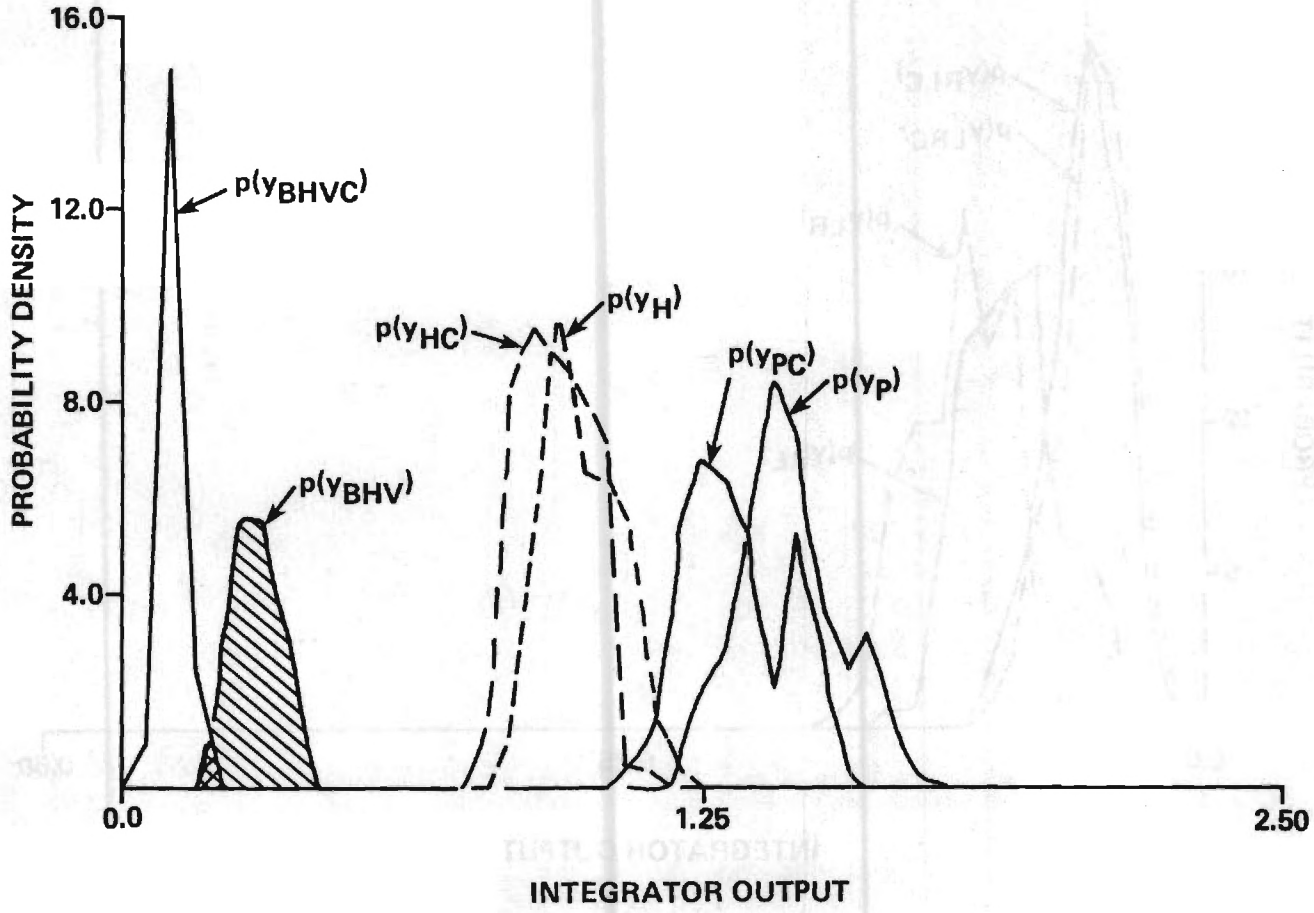

FIGURE 3–6. PROBABILITY DENSITY FUNCTIONS FOR INTEGRATOR OUTPUTS DEFINED IN FIGURE 3–1. (SCR = –8.8 dB).

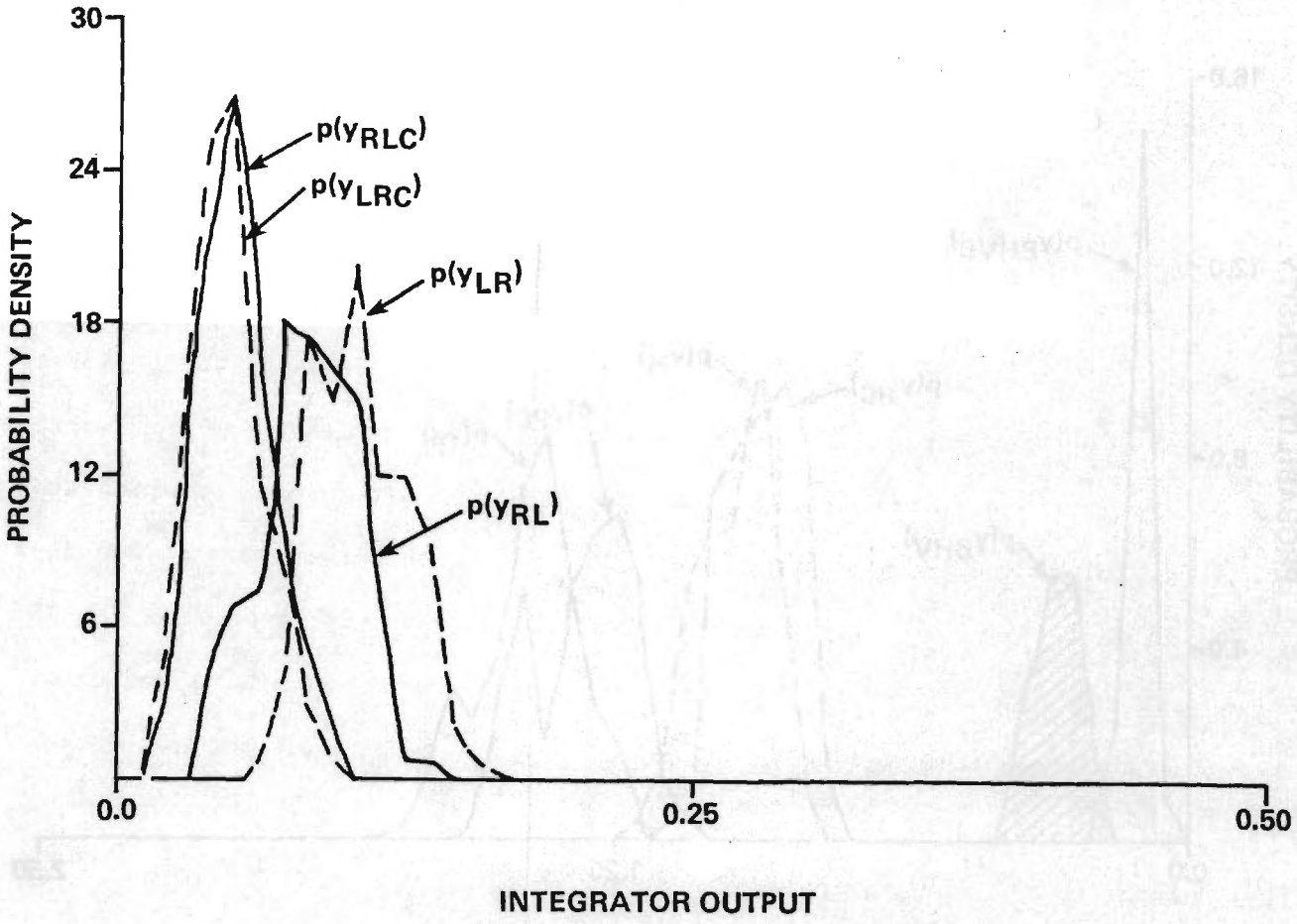

FIGURE 3–7. PROBABILITY DENSITY FUNCTIONS FOR INTEGRATOR OUTPUTS FROM ORTHOGONAL CIRCULAR POLARIZATION ANTENNA CHANNELS. (SCR = –8.8 dB).

$$P_D = \int_T^\infty P_y(y)dy = \text{Probability of detection} \tag{6a}$$

$$P_{FA} = \int_T^\infty P_{yc}(y)dy = \text{Probability of false alarm} \tag{6b}$$

In the above equations, p_{yc} and p_y represent the pdf's for the clutter-only and targer-in-clutter cases, respectively. The lower limit of integration T is a suitably selected threshold which minimizes P_e over the range of SCR's expected; in the case at hand, -8.8 dB $\leq$ SCR $\leq$ .75 dB. The thresholds used to compute the P_e are shown in Figure 3-8.

The conventional power variables y_V, y_H, y_P demonstrate the worst performance in Figure 3-8. The LHC/RLC processor exhibits the next worst performance. (The two variables y_{LR} and y_{RL} were never combined and indicated in Figure 3-1 to provide discrimination between target and decoy.) Variables y_1 and y_2 use windowed, total received power with $\gamma = .78$ as indicated in Figure 3-1. Some improvement in performance is indicated in this case compared to the conventional case (y_V,y_H,y_P). But the processor which exhibits the best performance is the sin β_{HV} processor, where the input to the integrator is

$$V_{BHV} = V_V V_H |\sin \beta_{HV}| \tag{7}$$

The computed probability of error was essentially zero.

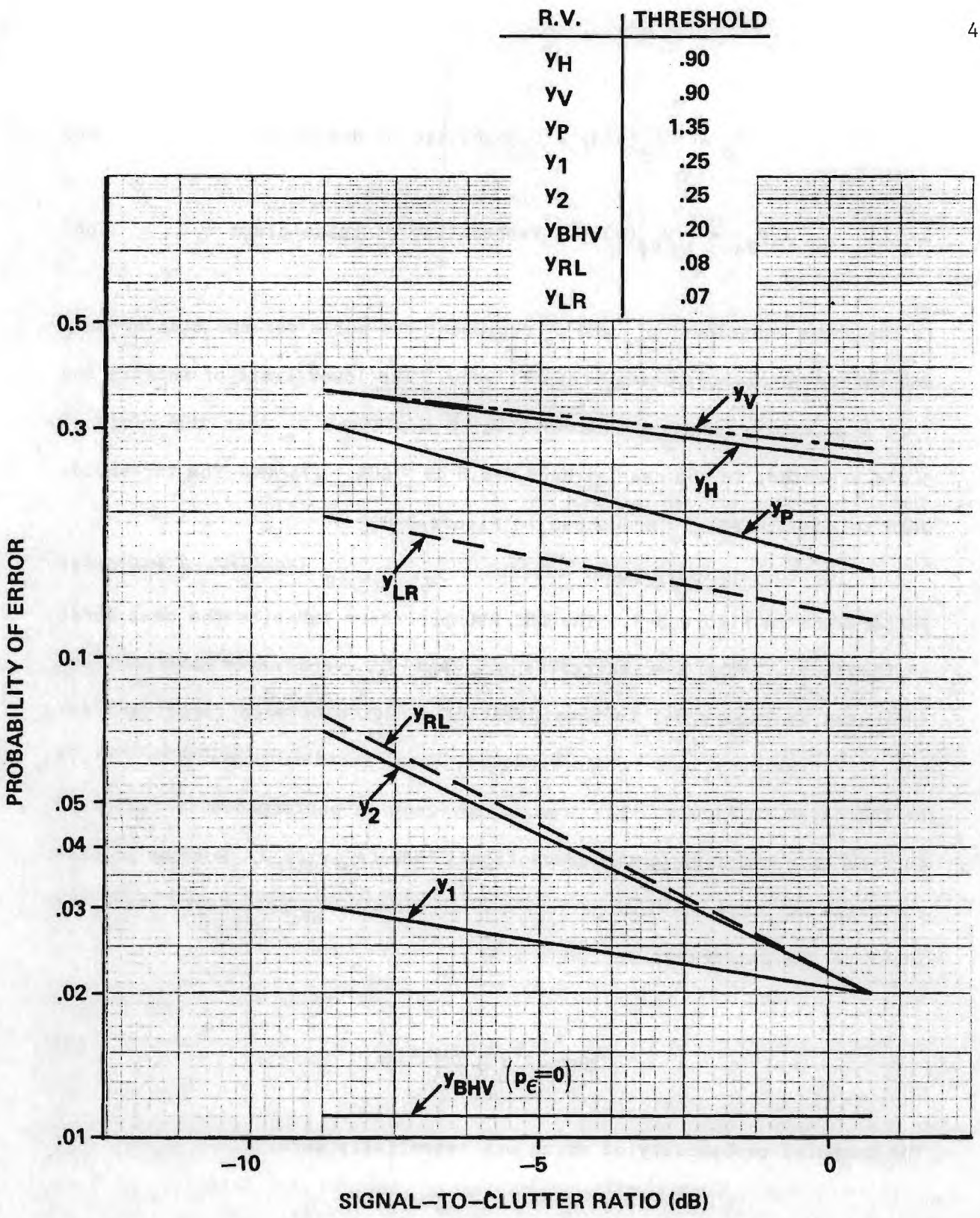

FIGURE 3–8. PROBABILITY OF ERROR VERSUS SIGNAL–TO–CLUTTER RATIO FOR EIGHT RANDOM VARIABLES DEFINED IN FIGURE 3–1.

CHAPTER 4

CONCLUSIONS AND RECOMMENDATIONS

Subject to the assumptions made regarding the statistics of the polarimetric scattering as presented in Figure 2-3, the sin β_{HV} processor is superior to all other processors considered. This conclusion corroborates a view long held by many investigators in this field. Unfortunately, detractors will certainly claim that the scattering models are contrived.

No conclusions can be made concerning the validity of the scattering models used in the simulations; hence, it is recommended that available, measured polarimetric data at the frequencies of interest be processed to quantify the statistics of the polarimetric scattering. If such data are not available, it is recommended that a measurements program be undertaken to accumulate such data. Once the statistics of the scattering are known, it is recommended that the scattering models be enhanced to reflect those statistics so that valid simulations can be done.

The data and simulation results presented in this report pertain only to signals received in the sum mode of the assumed monopulse antenna. The performance of the angle tracking part of the radar has yet to be assessed when polarimetric processing is used. It is recommended that simulations be done using the scattering models of Figure 2-4 to assess the angle tracking performance of monopulse antennas using basically the processing schemes presented in Figure 3-1. While the validity of such simulations will be subject to the same constraints now present, the results will help identify the major areas of concern and to help identify the best parameters to use in the tracking algorithms. As better statisti-

cal models become available, they can be incorporated into the simulations as developed at that point in time.

Once these necessary simulation tools are developed and verified, they can be used to assess the effects of radomes and polarizers on the performance of the polarimetric processing radar antenna. It will be of particular interest to identify any polarizer functions which would enhance processor performance or produce better target discriminants.

Additional research is also recommended to utilize the polarization nulls of targets and clutter in the target detection process. At present, the use of LHC polarization may not be optimum; i.e., other polarizations may provide a better target discriminant. Any measurements programs carried out should give due consideration to the general nature of the polarization scattering matrix, especially with regard to variables to be measured and the conditions of the experiments performed. Properly performed experiments will provide valid data that can serve a variety of purposes and need not be restricted to a single processing scheme or application.

The importance of validating the hypothesized nature of polarimetric scattering cannot be over emphasized. No scientifically valid assessments of the merits of polarimetric processing can be made until the statistics of the scattering process are adequately quantified.

REFERENCES

[1] G. K. Huddleston, H. L. Bassett, and J. M. Newton, "Parametric Investigation of Radome Analysis Methods: Computer-Aided Radome Analysis Using Geometrical Optics and Lorentz Reciprocity," Final Technical Report, Volume 2, Grant AFOSR-77-3469, February 1981.

[2] Richard L. Mitchell, Radar Signal Simulation, Artech House, Inc., Delham, MA 02026, 1976.

[3] David K. Barton, Radar System Analysis, Prentice-Hall, Inc., New Jersey, 1964.

[4] S. Stein and J. J. Jones, Modern Communication Principles, McGraw-Hill, New York, 1967, Ch. 3.

[5] W. B. Davenport, Jr. and W. L. Root, Random Signals and Noise, McGraw-Hill, New York, 1958, Ch. 12.

[6] G. T. Ruck, D. E. Barrick, and W. D. Stuart, Radar Cross Section Handbook, Plenum Press, New York, 1970, Vol. I, Ch. 2.

[7] Bob Raven, "Simulation of Polarimetric Radar Target Extraction Performance," Proceedings of the Workshop on Polarimetric Radar Technology, GACIAC PR-81-02, June 1980, pp. 165-183.

[8] S. H. Bickel, "Some Invariant Properties of the Polarization Scattering Matrix," Proceedings IEEE, August 1965, pp. 1070-1072.

[9] W. M. Boerner, "Polarization Mircowave Holography: An Extension of Scalar to Vector Holography," Proceedings of 1980 S.P.I.E. Technical Symposium East, April 1980, paper no. 231-23, 11 pages.

[10] W. M. Boerner, "Use of Polarization in Electromagnetic Inverse Scattering," Proceedings of 1980 International Symposium on Wave Propagation, Munchen, FRG, August 1982, 5 pages.

[11] A. J. Poelman, "The Applicability of Controllable Antenna Polarizations to Radar Systems," Tijdschrift van het Nederlands Electronica en Radiogenootschap, 44, pp. 93-106, 1979.

[12] J. Richard Huynen, "Measurement of the Target Scattering Matrix," Proceedings IEEE, August 1965, pp. 936-946.

[13] J. Richard Huynen, "A New Approach to Radar Cross-Section Measurements," IRE International Convention Record, 10, pp. 3-11, 1962.

[14] L. W. Root, "The History of Polarimetric Radar Technology," Proceedings of the Workshop on Polarimetric Radar Technology, GACIAC PR-81-02, June 1980, pp. 1-14.

[15] D. A. Conner, "Pseudo-Random Number Generators Having Specified Probability Density Function and Autocorrelation," Ph.D. Thesis, School of Electrical Engineering, Georgia Institute of Technology, Atlanta, GA, 1971.

[16] F. E. Nathanson, Radar Design Principles, McGraw-Hill, New York, 1969.

[17] Peter Swerling, "Probability of Detection for Fluctuating Targets," RAND Corp., Research Memo RM-1217, March 17, 1954.